Bulgarian Society for NDT
**International Journal "NDT Days"**
Volume II, Issue 4, Year 2019
ISSN: 2603-4018
eISSN: 2603-4646

# Determination of Mechanical Properties of Paramagnetic Materials by Multi-frequency Method

Yuriy KALENYCHENKO, Victor BAZHENOV, Aleksandr KALENYCHENKO, Viktor KOVAL, Sergiy RATSEBARSKIY

National Technical University of Ukraine "Igor Sikorsky Kyiv Polytechnic Institute" (Igor Sikorsky Kyiv Polytechnic Institute), Kyiv, Ukraine,
e-mails: yuriykalenychenko@gmail.com, vgbazhenov@gmail.com, akalenychenko@gmail.com, department_5@ukr.net, fazzer6132@gmail.com

**Abstract**
A new multi-frequency eddy current method of non-destructive testing can be used for determination of relations between phase characteristics of polyharmonic signals with mechanical properties of paramagnetic materials, which was experimentally established in the presented researches. With this purpose an electronic digital system for measuring the amplitude-phase characteristics of response signals has been designed. Researches were conducted on a series of samples from the alloy AA2024 with different levels of plastic deformation. The results of experiments showed that the amplitude-phase characteristic of the response signal has a regularity in dependence with the applied influences on the investigated material and is an information feature that allows to determine the stress state of the material.

**Keywords**: multi-frequency method, polyharmonic signals, amplitude-phase characteristic, eddy current method, paramagnetic materials

## 1. Introduction

The rapid development of approaches to the design and production of materials, such as "Integrated Computational Materials Engineering" [3, 7], "Materials Genome Initiative" [2, 8], "Additive Technologies" [4, 5, 6], expects new methods for determining the properties of microstructures during their creation and subsequent exploitation [1].
It is well known that the microstructure of certain structural materials, such as alloys, depends on the defects of the crystals and affects mechanical properties such as strength, ductility, and toughness [1, 9]. Non-destructive testing (NDT) methods are used to determine the microstructure of materials, since they are well adapted for use in technological quality control operations. Magnetic methods [10, 11, 12], ultrasonic [13, 14, 15, 21], eddy current (EC) [16, 17, 18, 20], pulsed eddy current (PEC) [21, 25, 26, 27], thermography [19 22, 23, 24] have become the most widespread. The effectiveness of these methods increases through the use of multi-frequency techniques [28, 30] and spectral analysis [29, 30].
In the above methods, the amplitude, frequency, time domain are investigated. However, direct studies of the initial phases in higher harmonics of response signals have not been performed, although they are related to the amplitude, frequency and time.
In this report, the use of a eddy-current multi-frequency NDT method will be considered, the specifics of which is that for the first time phase characteristics of response signals higher harmonics are used for studying the microstructure by a specifically designed measuring system (hereinafter in case the term "harmonic" is referred to a specific higher harmonic, the abbreviation "HX" (H- a higher harmonic, "X" – a harmonic number) is used.

## 2. Measuring system

For experiments, there has been developed a measuring system "Structuroscope EG", which determines the amplitude-phase characteristics of the higher harmonics of response signals. The main units of the system (Fig. 1) are the following: an electronic unit (1), a sensor (2), and a computer (3).
The electronic unit (1) is intended for synthesis of excitation signals of a given configuration and processing of response signals. It contains a synthesizer of signals, digital-to-analog and analog-to-digital converters, a control module, memory modules, interfaces for connecting external devices, and a cascade of amplifiers. It is configured by the parameters of a sampling frequency, form, frequency, amplitude, excitation signal intervals, as well as automatic changes of these parameters during measurements by a given algorithm. There can be used sensors (2) of eddy-current, ultrasonic, optical NDT in the measuring system. Using the computer (3) the configuration of the measuring system can be changed and adjusted depending on the characteristics of the object under control, the sensor, and also the research tasks.

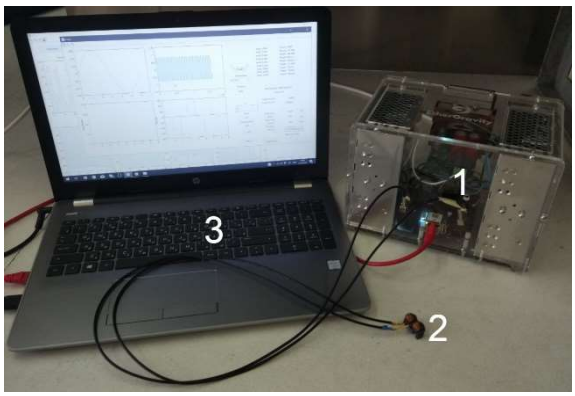


**Fig. 1. Structuroscope EG**

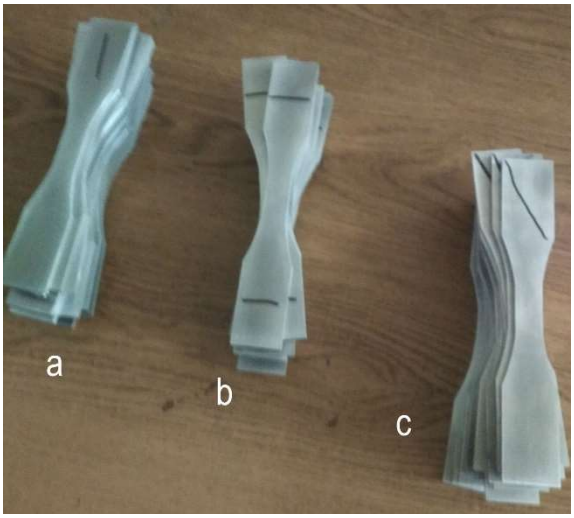


**Fig. 2. Samples to stretch: "along" (a), "across" (b) and at an angle $45^0$ (c) in relation to the rolling direction**

## 3. Materials and samples

For experiments, the sheet material of 3*mm* thickness from the AA2024-T4 alloy has been selected, which after its natural exposure to a stable temper has an optimal combination of properties (strength, toughness, and corrosion resistance), that is why it is widely used in industry, including aerospace [1]. Both industry and science have a wide experience of testing products from alloys of AA2HXX series using various NDT technologies and methods.
Since it is well-known that the viscoelastic response of structural materials is directly related to the microstructure [1, 9], the relation between microstructure and response signals phase characteristics was investigated on samples with different levels of plastic strain, obtained by applying to samples an axial load test, and samples themselves were prepared "along", "across" and at an angle $45^0$ in relation to the rolling direction. A general view of the samples is shown on Fig. 2.

The axial load test was carried out on the test bench BiSS-02-112, which allows to measure the length of the longitudinal effort with a relative error of 1%. A strain gauge with a base of 25*mm* was used to determine the strain, the measurement error of nonlinearity at the same time did not exceed 1%. The frequency of recording (fixing) the experimental data was 6 counts per second. During the tests, the samples were exposed to loads, resulting in deformation within the range from 0 to the deformation corresponding to the material ultimate strength which is characterized by different levels of their plastic component.
The Fig. 3 shows the Stress-Strain Curve for the samples "along" (code 00) and "across" (code 90) the rolling direction. Table 1 shows the strass/strain data for plastic deformation of various samples, which were subsequently used to establish a relation between microstructure and response signals phase characteristics.

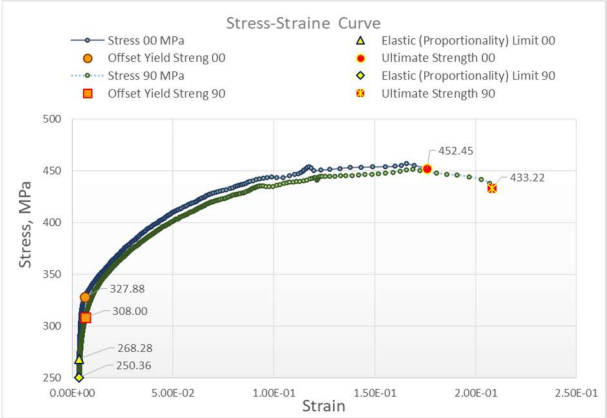


**Fig. 3. Stress-Strain Curve for samples "along" (code 00) and "across" (code 90) rolling directions**

**Table 1. Data Stress-Strain**

| Sample Code | Max Stress, MPa | Max Strain |
|---|---|---|
| AA2024.90.05 | 266,8806 | 3,80E-03 |
| AA2024.90.04 | 266,9685 | 3,57E-03 |
| AA2024.00.06 | 294,7953 | 4,15E-03 |
| AA2024.00.04 | 323,4991 | 6,44E-03 |
| AA2024.90.07 | 336,9895 | 1,40E-02 |
| AA2024.90.06 | 337,1025 | 1,46E-02 |
| AA2024.00.08 | 343,2031 | 1,48E-02 |
| AA2024.00.07 | 353,4626 | 1,36E-02 |
| AA2024.00.10 | 376,0512 | 3,26E-02 |
| AA2024.90.09 | 376,7396 | 3,41E-02 |
| AA2024.90.08 | 376,7814 | 4,24E-02 |
| AA2024.00.09 | 391,3189 | 3,32E-02 |
| AA2024.90.11 | 407,7242 | 5,72E-02 |
| AA2024.90.12 | 421,0229 | 7,56E-02 |
| AA2024.90.10 | 426,2230 | 1,04E-01 |
| AA2024.00.12 | 432,1944 | 7,80E-02 |
| AA2024.90.13 | 444,2872 | 1,26E-01 |
| AA2024.00.14 | 448,2887 | 1,13E-01 |
| AA2024.00.16 | 455,8687 | 1,42E-01 |
| AA2024.00.17 | 456,3806 | 1,49E-01 |

# 4. Experiments

## *4.1 Method*

The synthesized sinusoidal signal of the given parameters is fed to the sensor excitation winding made on the basis of a ferrite core. The excitation signal and the sensor windings parameters are selected in such a way that due to the nonlinear characteristics of the ferrite it is possible to produce a poly-harmonic electromagnetic field in a sample that excites a spectrum of harmonics of eddy currents of the corresponding frequency. As a result, in the measuring winding there is induced a spectrum of response signals, which is the coherent to the analog-to-digital converters sampling frequency, which allows to determine the initial phases values of the response signals harmonics.

A stepwise increase in the excitation signal amplitude causes the change in response signals harmonics amplitudes and initial phases (Fig. 4), and the character of such changes, in particular of the initial phases, is associated with the physical and mechanical characteristics of the object under control.

In Section 4.2, the research of the relation between the higher harmonics initial phases changes in the response signals and the levels of plastic deformation of the samples from the material AA2024-T4 is presented.

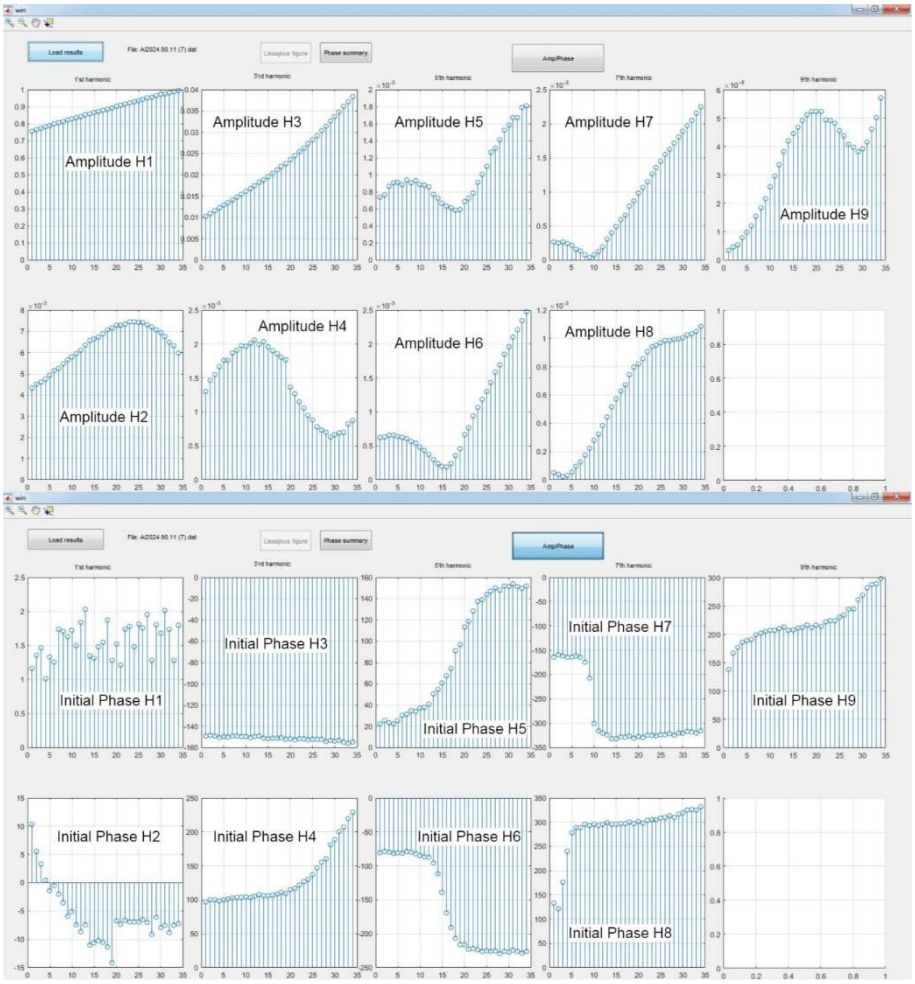


**Fig. 4. Changing the response signals value of the amplitudes and the initial phases of the harmonics, depending on the change in the excitation signal amplitude**

### *4.2 Research*

The report presents for the first time the results of measuring the initial phases of response signals higher harmonics. The measurement operations are carried out in automatic mode with a stepwise increase of the excitation signal by a given step of amplitude change from the value of $A_1$ to the value of $A_2$, the ratio $A_1/A_2 = 1{,}16$.

For each sample, there were nine different sensors taken to perform over 100 measurements, which determined the most acceptable parameters of the sensor and the excitation signal for measuring the initial phases of higher harmonics. The report presents the results of two series of measurements: the first one was executed on 14.02.2019 and 15.02.2019 by Sensor 5, the second one – on 19.04.2019 by Sensor 9. The both mentioned sensors have the same ferrite core, however, in order to provide different maximum values of the excitation signal current, the parameters of the excitation and measuring windings are taken different. The Sensor 9 maximum excitation current is 7 times more of the Sensor 5 maximum excitation current. In both series, identical parameters of sampling frequency, harmonic frequency, number and duration of intervals of synthesized excitation signal of sinusoidal shape were established, while the values of current differed.

For each item of the sample, there was received within the measurement cycle a spectrum of the response signals initial phases, which change due to an increase in the amplitude of the excitation signal. Fig.6 shows an example of change in the phases spectrum of nine harmonics of the sample AA2024.90.13 measured by the Sensor 9, where the X axis is the number of the measurement interval, and the Y axis indicates the value of the harmonic initial phase in degrees, and Fig.5 shows changes in the phase spectrum of the Sensor 9 without sample. In order to provide the statistical control over measured values of the initial phases in measurements with the Sensor 5 there were ten cycles performed, and with the Sensor 9 – six cycles of measurements for each sample. Also there was control of external parameters of the working environment, in particular, temperature of samples, sensors, electronic components of the device, positioning of the sensor on the samples. The statistical control of the measurement process was established using the Moving Range (MR) Chart [31].

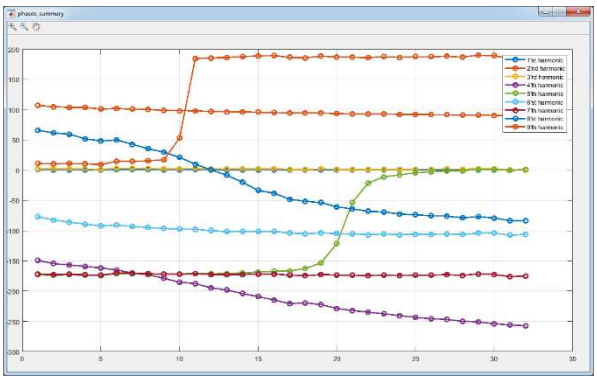

**Fig. 5. Sensor 9 without Samples: dependence of the phases spectrum of 9 response signal harmonics of increasing the amplitude of the excitation signal**

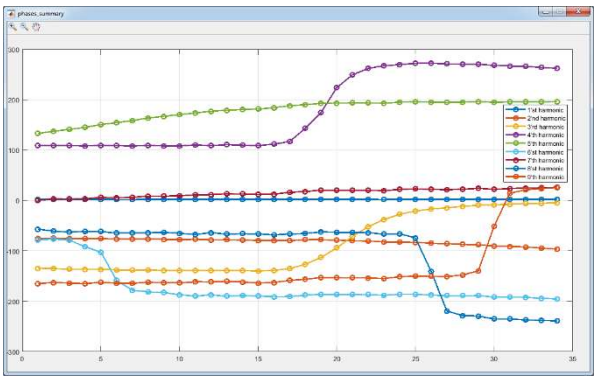

**Fig. 6. Sensor 9, Sample AA2024.90.13, dependence of the phases spectrum of 9 response signal harmonics of increasing the amplitude of the excitation signal**

The results of measurements showed a high reproducibility for higher harmonics, which in most cycles completely fit into the confidence interval (CI) – Fig.10, Fig.12, however, H1 always

had variations in the values of the initial phase that are beyond the limits of the lower control limit (LCL) / upper control limit (UCL) – Fig.7 [31].
The measured data were processed using a graphical analysis of the dependence of the response signal harmonic initial phase change from the growth of the excitation signal amplitude stages. Fig.7–Fig.20 show examples of graphs of this dependence prepared by means of MATHLAB in automatic mode, where the X axis shows the reduced ratio of the response signal amplitude H1 to the magnitude of the stepwise increase of the excitation signal, which did not change during all measuring cycles, and the axis Y indicates the value of the harmonic initial phase in degrees.

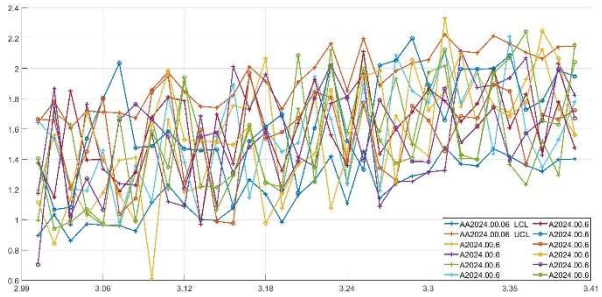

**Fig. 7. Sensor 5, Sample AA2024.00.06: variations of the H1 initial phase $10^s$ measurements cycles of response signal and LCL/UCL**

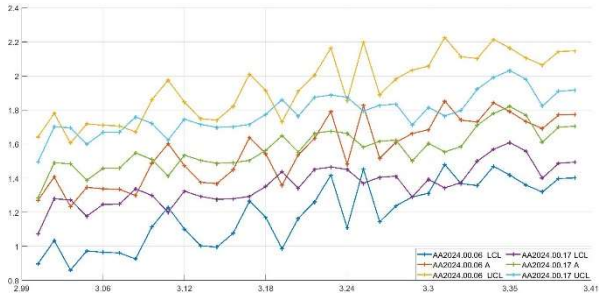

**Fig. 8. Sensor 5 – Samples AA2024.00.06, AA2024.00.17: Average initial phase of H1 response signal and LCL/UCL**

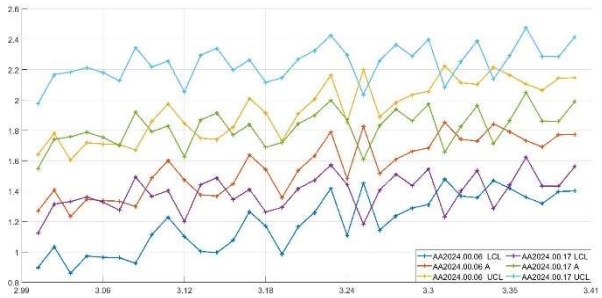

**Fig. 9. Sensor 5 – Sample AA2024.00.06, Sensor 9 – Sample AA2024.00.17: Average initial phase of H1 response signal and LCL/UCL**

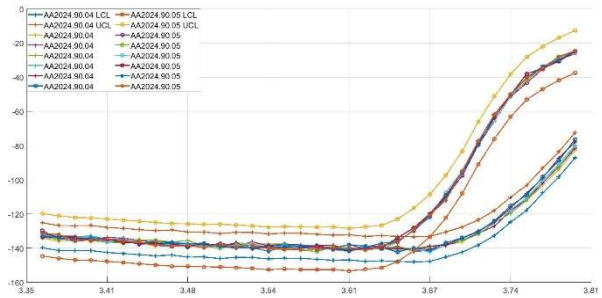

**Fig. 10. Sensor 9 – Samples AA2024.90.04, Sample AA2024.00.17: variations of the H3 initial phase $6^s$ measurements cycles of response signal and LCL/UCL**

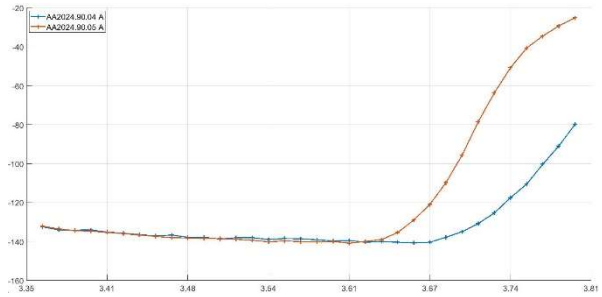

**Fig. 11. Sensor 9 – Samples AA2024.90.04, Sample AA2024.00.17: H3 average initial phase $6^s$ measurements cycles of response signal**

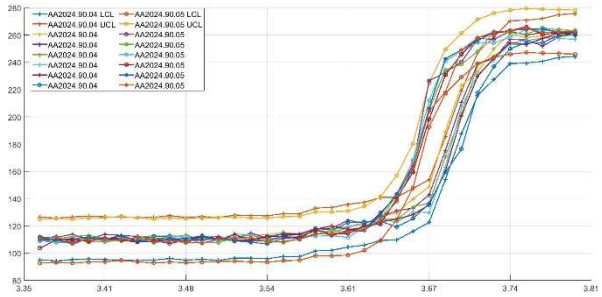

**Fig. 12. Sensor 9 – Samples AA2024.90.04, Sample AA2024.00.17: variations of the H4 initial phase $6^s$ measurements cycles of response signal and LCL/UCL**

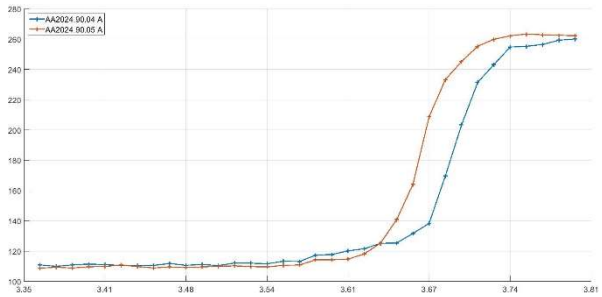

**Fig. 13. Sensor 9 – Samples AA2024.90.04, Sample AA2024.00.17: H4 average initial phase $6^s$ measurements cycles of response signal**

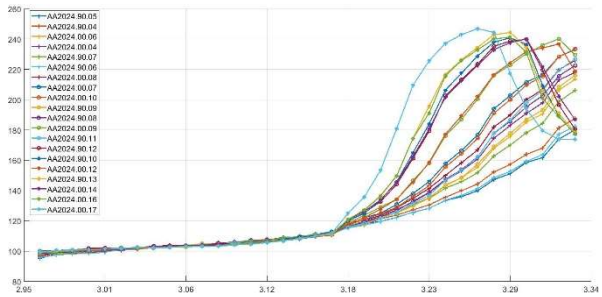

**Fig. 14. Sensor 5 – all Samples: H4 average initial phase $10^s$ measurements cycles of response signal**

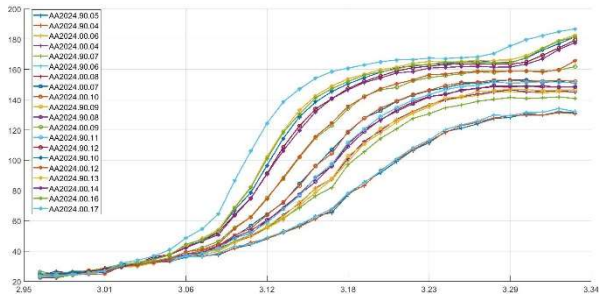

**Fig. 15. Sensor 5 – all Samples: H5 average initial phase $10^s$ measurements cycles of response signal**

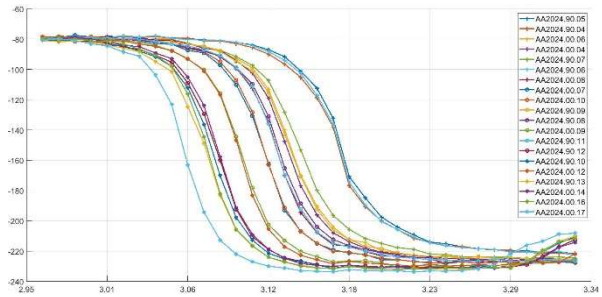

**Fig. 16. Sensor 5 – all Samples: H6 average initial phase $10^s$ measurements cycles of response signal**

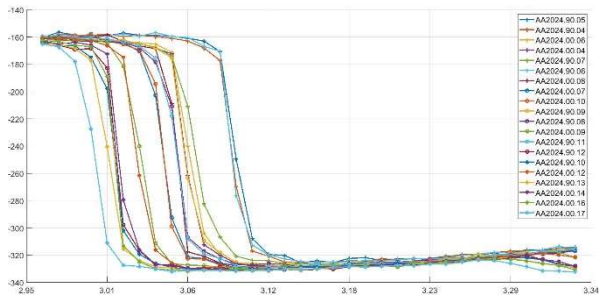

**Fig. 17. Sensor 5 – all Samples: H7 average initial phase $10^s$ measurements cycles of response signal**

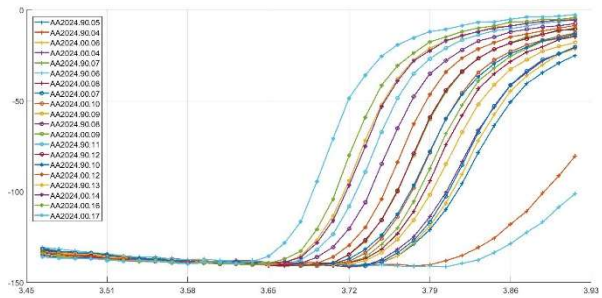

**Fig. 18. Sensor 9 – all Samples: H3 average initial phase $6^s$ measurements cycles of response signal**

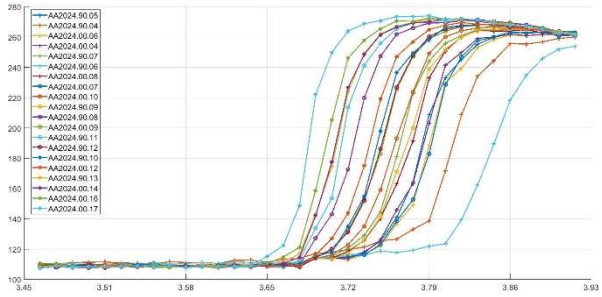

**Fig. 19. Sensor 9 – all Samples: H4 average initial phase $6^s$ measurements cycles of response signal**

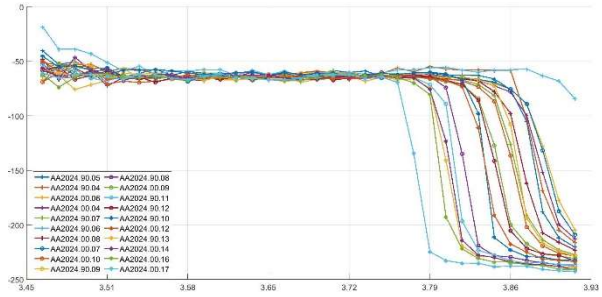

**Fig. 20. Sensor 9 – all Samples: H8 average initial phase $6^s$ measurements cycles of response signal**

The dependencies shown on Fig.7–Fig.20 indicate that at some parameters of the excitation signal amplitude, the initial phases of the higher harmonics for different specimens vary within several tens of degrees and do not differ in their values, but at certain parameters of the excitation signal, they begin to change rapidly within the hundreds of degrees (harmonics H3 and higher), at that the initial phase of each sample varies to a different extent from the other samples in the areas of rapid changes. So far, the authors of the report couldn't find the explanation of the differences in the initial phases for various samples, however, it is observed that the curves of rapid change initial phase for samples with lower stress tend to be "to the right" on the charts, with average values of stress – in the middle, and with higher stresses – "to the left". In order to determine the regularity of the differences, it is planned to conduct a study of the phase characteristics for new samples subjected to various types of mechanical tests, with preliminary (before tests) obtaining phase characteristics of the sheet material and samples made from it, as well as defining the microstructure characteristics at all stages of the study by means of the electron backscattering diffraction technique and scanning electron microscopy [32].

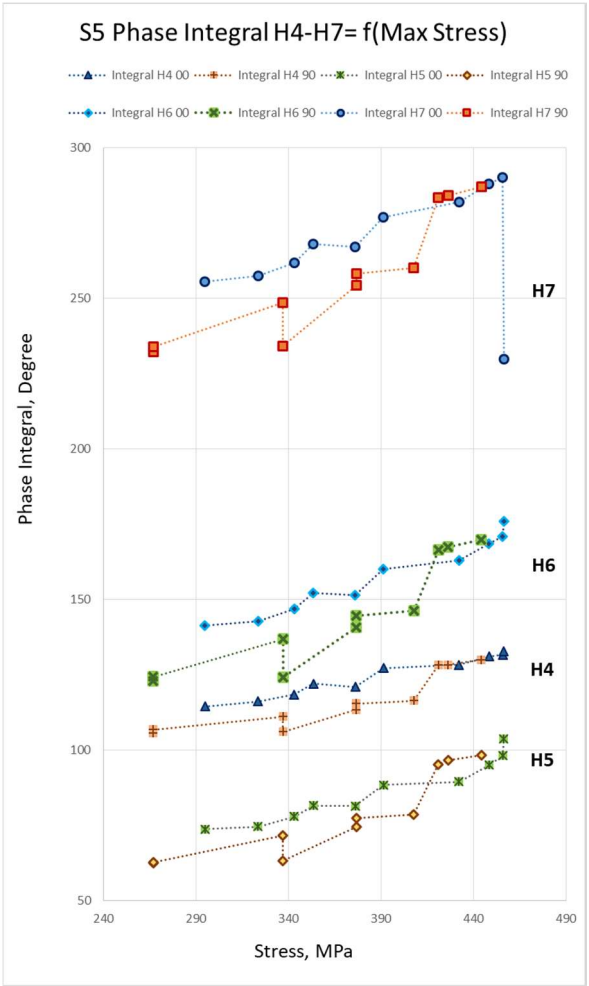


**Fig. 21. Sensor 5 – all Samples: dependence of the H4, H5, H6, H7 initial phase of the response signal with the stress**

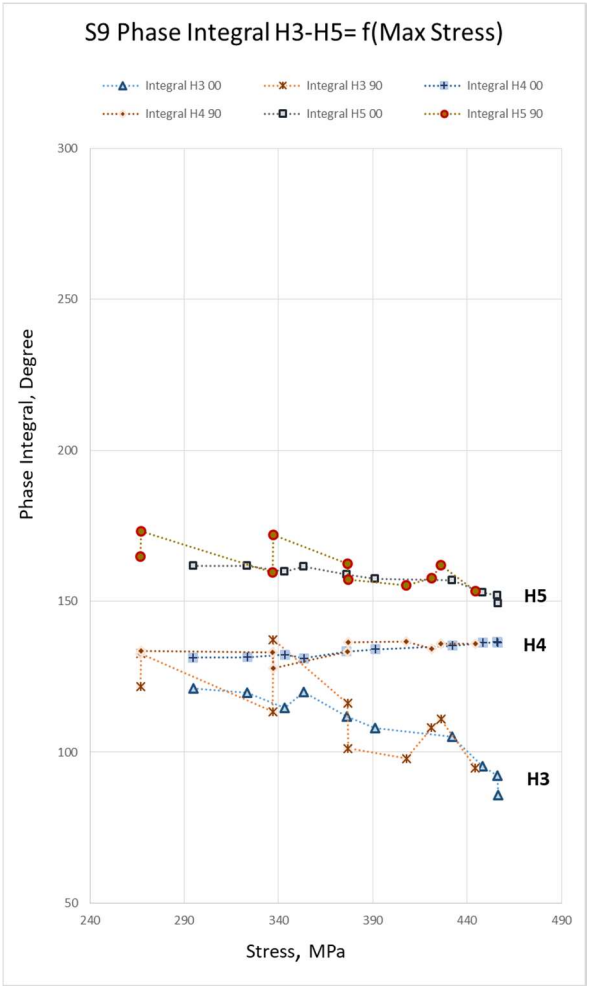


**Fig. 22. Sensor 9 – all Samples: dependence of the H3, H4, H5 initial phase of the response signal with the stress**

In order to establish the relationship between the phase characteristics of the stressed samples the Phase Integral HX = f (Max Stress) (Fig.21, Fig.22) was built by using an integral

calculation of the initial phase spectra, where the Phase Integral HX (PI) is the initial phase change integral of X-th harmonic from the given amplitude of excitation, Max Stress – maximum stress applied to a sample during simple stretching (Table 1). Points on the graphs are the values of the sample PI, and dotted lines between the points indicate the sequence of growth of stress values (in Table 1, samples are sorted by increasing stress). It is observed that the change of PI have a nonlinear dependence, the change of samples PI with the code 00 (along the direction of rolling) differs from the change of samples PI with the code 90 (across the direction of rolling), while the graphs of change in the samples PI of 00 code for Sensors 5 and 9 are similar, as well as those for code 90 respectively. Also, the modified laws have some correlation with the Strain-Stress Curve (Fig.3). The choice of H4-H7 for the Sensor 5 and H3-H5 for the Sensor 9 was made subject to the statistical control over the values of the initial phases and the completion of the process of their rapid change.

### *4.3 Experimental Results*

Analysis of the received dependencies of the induced in the Structuroscope EG measuring system sensor winding amplitudes and phases changes demonstrates the following.

- The amplitude of the response signal H1 varies linearly with the change in the excitation signal (Fig. 4, Image Amplitude H1), actually reproducing the regularity of its change, at that no interaction between the excitation signal and the object under control is observed.
- The initial phase of the response signal H1 increases throughout the amplitude range of the excitation signal within the range of $0{,}5^0$, while the moving range – within $0{,}7^0$, the variation of its values is statistically uncontrolled (Fig. 7: the values are beyond the limits of the moving range) [31], which makes it impossible to detect distinct information features for samples with different plastic deformation: for example, Fig. 8 shows the average values and LCL/UCL for samples AA2024.00.06 and AA2024.00.17, measured by Sensor 5, and on Fig. 9 are shown the average values and LCL/UCL for the sample AA2024.00.06 measured by Sensor 5 and AA2024.00.17 measured by Sensor 9.
- The response signals higher harmonics amplitudes, depending on the object under control, may vary according to a complex law that differs from the law of the excitation signal amplitude change, and their magnitudes are used as one of the main information features in studying characteristics of the object under control in multi-frequency methods [30].
- The higher harmonics phases changes in relation to the excitation signal amplitude change also shows a complex dependence, and these changes are significantly sensitive to changes in the material under control microstructure than those in the amplitude. For example, the change in the initial phases of some harmonics during the growth of the excitation signal at certain values of its amplitude can reach hundreds of degrees: from $100^0$ to $250^0$ for Sensor 5, H4 (Fig.14), from $20^0$ to $160^0$ for Sensor 5, H5 (Fig.15), from $-80^0$ to $-230^0$ for Sensor 5, H6 (Fig.16), from $-160^0$ to $-330^0$ for Sensor 5, H7 (Fig.17), from $-140^0$ to $0^0$ for Sensor 9, H3 (Fig.18), from $110^0$ to $270^0$ for Sensor 9, H4 (Fig.19), from $-50^0$ to $-240^0$ for Sensor 9, H8 (Fig.17). The moment such stepwise changes appear in the initial phase depending on the excitation signal allows to establish the relation between the phase characteristics of the response signals and the microstructure of the object under control. The authors of the report assume that the effect of stepwise changes in the initial phases is related to the phenomena of electrons scattering due to the microstructural features of materials such as their morphology, the degree of recrystallization, grain size distributions and texture, and the second phases (precipitates, dispersoids, and constituents), grain-boundary corrosion, defects of crystal grids, and macrodefects [1, 9].
- The analysis of response signals higher harmonics phase information characteristics at changing the excitation signal amplitude turns out to be a very sensitive tool for determining the characteristics of the object under control material microstructure. As a result of the

research it was found that in order to study the characteristics of certain materials, there can be selected excitation parameters and harmonics which provide maximum sensitivity and accuracy for controlling the given mechanical parameters of the material and are measured within one iteration, which in turn will significantly reduce the time in the process of industrial application.

– The presented system of structuroscopy is developed to be reconfigurable, digital and fully automatic, it can be tuned to different modes of operation and presentation of measurement results, has small sizes, efficient power consumption, and is easy to use. The measurement cycle time in the laboratory, when the data package for 60 excitation signal values is received, does not exceed one minute. For industrial application when there is no need to investigate a wide range of changes in the excitation signal, the measurement cycle time will be minimized to a few seconds.

## 5. Acknowledgements

The authors express their sincere acknowledgement to private individuals who have financially supported the development of the "Structuroscope EG" measuring system and conducting researches.

### References

1. Krishnan K. Sankaran, Rajiv S. Mishra. Metallurgy and Design of Alloys with Hierarchical Microstructures. Elsevier, 2017, p. 506.
2. Anubhav Jain, Shyue Ping Ong, Geoffroy Hautier, Wei Chen, William Davidson Richards, Stephen Dacek, Shreyas Cholia, Dan Gunter, David Skinner, Gerbrand Ceder, Kristin A. Persson. Commentary: The Materials Project: A materials genome approach to accelerating materials innovation. APL Materials, Vol. 1, No. 011002, 2013.
3. Allison, J., Backman, D. & Christodoulou, L. Integrated computational materials engineering: A new paradigm for the global materials profession. JOM, Vol. 58, No. 25, 2006, pp 25–27.
4. F. Calignano, D. Manfredi, Elisa P. Ambrosio, Sara Biamino, Mariangela Lombardi, Eleonora Atzeni, Alessandro Salmi, Paolo Minetola, L. Iuliano, P. Fino. Overview on Additive Manufacturing Technologies. Proceedings of the IEEE, Vol. 105, No. 4, 2017, pp. 593 – 612.
5. Kaufui V. Wong, Aldo Hernandez. A Review of Additive Manufacturing. ISRN Mechanical Engineering, 2012
6. X. Lu. Remarks on the recent progress of Materials Genome Initiative. Sci. Bull., Vol. 60, No. 22, 2015, pp 1966–1968.
7. M. F. Horstemeyer. Integrated Computational Materials Engineering (ICME) for Metals: Using Multiscale Modeling to Invigorate Engineering Design with Science. Wiley-TMS, 2012, p 472.
8. David L. McDowell, Surya R. Kalidindi. The materials innovation ecosystem: A key enabler for the Materials Genome Initiative. MRS Bulletin, Vol. 41, No. 4, 2016, pp 326-337.
9. Ed. David E. Laughlin, Kazuhiro Hono. Physical Metallurgy. 5th Edition ed., Elsevier, 2015, p 2960
10. Kashefi, M., Kahrobaee, S. & Nateq, M.H. On the Relationship of Magnetic Response to Microstructure in Cast Iron and Steel Parts. Journal of Materials Engineering and Performance, Vol. 21, No. 7, 2012, p. 1520–1525
11. S. Ghanei, M. Kashefi, M. Mazinani.Comparative study of eddy current and Barkhausen noise nondestructive testing methods in microstructural examination of ferrite–martensite dual-phase steel."Journal of Magnetism and Magnetic Materials, Vol. 356, 2014, pp 103.
12. G. Vértesy, I. Mészáros, I. Tomášc. Nondestructive magnetic characterization of TRIP steels. NDT & E International, Vol. 54, 2013, pp 107-114
13. Aghaie-Khafri, M., Honarvar, F. & Zanganeh, S. Characterization of Grain Size and Yield Strength in AISI 301 Stainless Steel Using Ultrasonic Attenuation Measurements. Journal of Nondestructive Evaluation, Vol. 31, No. 3, 2012, pp 191-196.
14. S. E. Kruger, G. Lamouche, D. Lévesque and J.-P. Monchalin. Method and system for determining material properties using ultrasonic attenuation. United States Patent US7353709B2, 06.07.2005.

15. T. Kundu, Ed. Ultrasonic and Electromagnetic NDE for Structure and Material Characterization: Engineering and Biomedical Applications. 1st Ed., CRC Press, 2012, p. 890.
16. M Zergoug, S Lebaili, H Boudjellal, A Benchaala. Relation between mechanical microhardness and impedance variations in eddy current testing. NDT & E International, Vol. 37, No. 1, 2004, pp 65-72.
17. Tonghua Liu,Wei Wang,Wenjiang Qiang,Guogang Shu. Mechanical properties and eddy current testing of thermally aged Z3CN20.09M cast duplex stainless steel. Journal of Nuclear Materials, Vol. 501, 2018, pp 1-7.
18. S. Ghanei, M. Kashefi, M. Mazinani. Comparative study of eddy current and Barkhausen noise nondestructive testing methods in microstructural examination of ferrite–martensite dual-phase steel. Journal of Magnetism and Magnetic Materials, Vol. 356, 2014, pp 103-110.
19. Yunze He, Ruizhen Yang. Eddy Current Volume Heating Thermography and Phase Analysis for Imaging Characterization of Interface Delamination in CFRP. IEEE Transactions on Industrial Informatics, Vol. 11, No. 6, 2015, pp 1287-1297.
20. Abla Dahia, Eric Berthelot, Yann Le Bihan, Laurent Daniel. A model-based method for the characterisation of stress in magnetic materials using eddy current non-destructive evaluation. Journal of Physics D: Applied Physics, Vol. 48, No. 19, 2015.
21. A Habibalahi, M S Safizadeh. Pulsed eddy current and ultrasonic data fusion applied to stress measurement. Measurement Science and Technology. Vol. 25, No. 5, 2014.
22. Jia Liu, Wenwei Ren, Gui Yun Tian, Bin Gao, Yizhe Wang, Jishan Zhang, Brian Shaw, Aijun Yin, Naomi Omoyeni King-Alaleю Nondestructive Evaluation of Early Contact Fatigue Using Eddy Current Pulsed Thermography. IEEE Sensors Journal, Vol. 15, No. 8, 2015, pp 4409-4419.
23. Yunze He, Ruizhen Yang, Hong Zhang, Deqiang Zhoud, Gang Wange. Volume or inside heating thermography using electromagnetic excitation for advanced composite materials. International Journal of Thermal Sciences, Vol. 111, 2017, pp 41-49.
24. Carosena Meola, Giovanni M. Carlomagno, Luca Giorleo. The use of infrared thermography for materials characterization. Journal of Materials Processing Technology, Vol. 155-156, 2004, pp 1132-1137.
25. M. Zergoug, N. Boucherrou, A Hammouda, G.Kamel. Characterization of multilayer corrosion by pulsed eddy current. 3rd MENDT – Middle East Nondestructive Testing Conference & Exhibition, Bahrain, Manama, 2005.
26. Liang Cheng and Gui Yun Tian. Comparison of Nondestructive Testing Methods on Detection of Delaminations in Composites. Journal of Sensors, Article ID 408437, 2012 p 7.
27. Gui Yun Tiana, Yunze Hec, Ibukun Adewalea, Anthony Simma. Research on spectral response of pulsed eddy current and NDE applications. Sensors and Actuators A: Physical, Vol. 189, pp. 313-320, 15 January 2013
28. W. Yin, A.J. Peyton. Thickness measurement of non-magnetic plates using multi-frequency eddy current sensors. NDT & E International, Vol. 40, No. 1, 2007, pp 43-48, January.
29. Yunze He, Mengchun Pan, Feilu Luo, Guiyun Tian. Pulsed eddy current imaging and frequency spectrum analysis for hidden defect nondestructive testing and evaluation. NDT & E International, Vol. 44, No. 4, 2011, pp 344-352.
30. Ali Sophian, Guiyun Tian, Mengbao Fan. Pulsed Eddy Current Non-destructive Testing and Evaluation: A Review. Chinese Journal of Mechanical Engineering, Vol. 30, No. 122, 2017, pp 500–514.
31. Robert L. Mason, Richard F. Gunst, James L. Hess. Statistical Design and Analysis of Experiments: With Applications to Engineering and Science, Second Edition,.John Wiley & Sons, 2003, p. 760.
32. M. Alvand, M.Naseri, E.Borhani, H. Abdollah-Pourю Nano/ultrafine grained AA2024 alloy processed by accumulative roll bonding: A study of microstructure, deformation texture and mechanical propertiesю Journal of Alloys and Compounds, vol. 712, 2017 pp 517-525.